

Chapter 2

Super-Intense Laser-Plasma Interaction in Real-World Applications

Andrey Savel'ev, Konstantin Ivanov, Roman Volkov,
Sergei Shulyapov, Ivan Tsymbalov and Alexei Lar'kin

In my talk, I would like to address the issue of super-intense laser-plasma interaction in relation to some applications in fundamental and applied science with potential in biology, medicine, nuclear non-proliferation, etc. This is why we would like not to think of some huge laser machines which are needed to produce intensities above 10^{20} W/cm², but would like to deal with really table-top femtosecond lasers that can be installed in any university-scale laboratory quite easily.

The parameters of our tetawatt Ti:sapphire laser are: energy per pulse 1–50 mJ, pulse duration ~ 45 fs, central wavelength 805 nm, repetition rate 10 Hz with M^2 1.2–1.7. Figure 2.1 presents third-order correlation traces of our pulse in two configurations, and now we have also an XPW option, so the ultimate available contrast is some two orders of magnitude better.

The main activity of our laboratory is relativistic laser-plasma interaction with underdense plasma; with structured targets, we are trying to look at electron and ion

A. Savel'ev (✉) · K. Ivanov · R. Volkov · S. Shulyapov · I. Tsymbalov · A. Lar'kin
International Laser Center & Physics Faculty, M.V. Lomonosov Moscow State University,
GSP-1, Leninskie Gory 1, Bld. 62, Moscow 119991, Russia
e-mail: abst@physics.msu.ru

K. Ivanov
e-mail: akvonavi@gmail.com

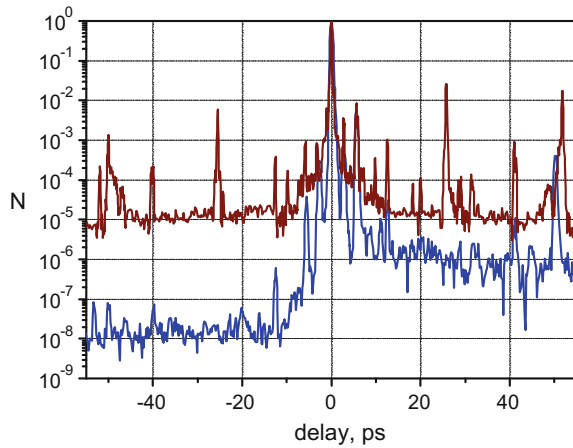
R. Volkov
e-mail: rv_volkov@phys.msu.ru

S. Shulyapov
e-mail: ser270489@ya.ru

I. Tsymbalov
e-mail: ivankrupenin2@gmail.com

A. Lar'kin
e-mail: alexeylarkin@ya.ru

Fig. 2.1 Third-order correlation traces of the terawatt femtosecond laser pulse for two different setups



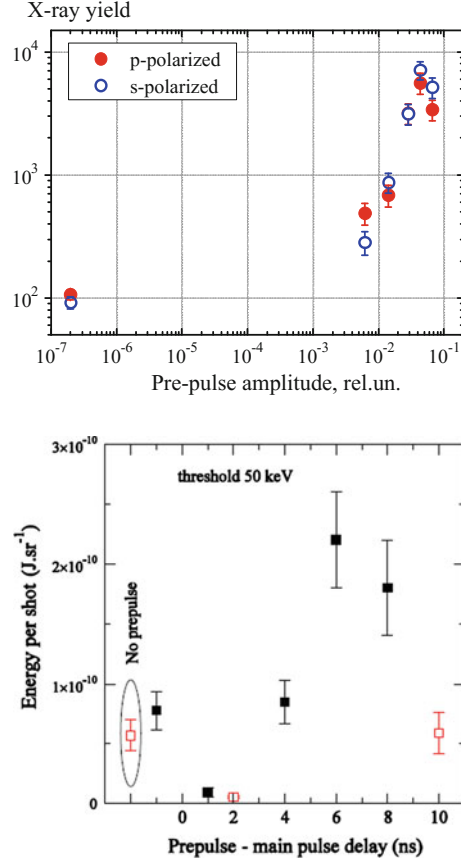
acceleration, and X-ray and γ production, and also we are working on laser-induced nuclear processes such as nuclear excitation, nuclear reaction, and so on, but I will not touch this topic in my talk. Also, we are working on femtosecond filamentation in gases and solids. Please refer to the talks by Prof. Kosareva and Prof. Shkurinov to get more details on this latter activity.

The following talk is divided by two parts. The first one deals with hard X-ray sources. It is not a good idea to use a simple solid target, because you need to move the target from shot to shot to have a clean, undamaged surface, and this task is quite complicated even at 10 Hz or at higher repetition rates, especially if you would like to use your source for hours.

We introduced a liquid-gallium target setup [1, 2], which has a lot of different advantages such as self-healing of the surface after laser action and extremely easy target setup (it does not contain any moving parts). For such a target, you can use various materials such as Ga, In, Bi, and Pb. They should have low-saturated vapor pressure, so you cannot use mercury. All these materials are metals, so they have high thermal conductivity, and this is also good (you cannot use water). But we are concentrated mostly on Ga because of its extremely low melting temperature, and so it is very nice to use it without some of the implications of the hot temperature inside the chamber.

First, we observed that we could work at 10 Hz or even at 1 kHz [3], i.e., we can produce stable hard X-rays without changing or moving something inside the chamber, and this is very nice for applications. Also, we observed very interesting physics inside, and that means that, if we play with short nanosecond pre-pulse coming 12 ns in advance of the main pulse (we can play with the amplitude of this pulse; we can play with advancing time of this pulse with respect to the main pulse), we significantly enhance the hard X-ray yield and the mean energy of hot electrons. For example, in Fig. 2.2, we plotted experimental data for Ga.

Fig. 2.2 Hard X-ray yield dependencies on the amplitude and advancing time of the pre-pulse. The main pulse intensity is 10^{17} W/cm². The latter dependence was measured in a collaborative experiment with CELIA [2, 4]



To get more insight into the physics, we made shadowgraphy measurements of the plasma plume created by the pre-pulse (Fig. 2.3) [2]. One can see here that there are something like jets, something like micro-structuring. So we assume that those micro jets are the main cause, and those micro jets are not produced by the main pulse but by the pre-pulse.

To understand physics inside this liquid jet generation, we have collaborated with Prof. Tikhonchuk's group from CELIA (University of Bordeaux), and one can see 2D hydrodynamic simulations in Fig. 2.4 [4]. From these simulations, it follows, that, if we assume inhomogeneous energy deposition on the target, we immediately come to microjet production.

Also, we checked in an experiment that the jet geometry closely correlates with energy distribution in the focal area [4], and we can play with energy distribution just by changing the focus position. Now we are trying to make some regular jets and to optimize jets to get even better and more stable results.

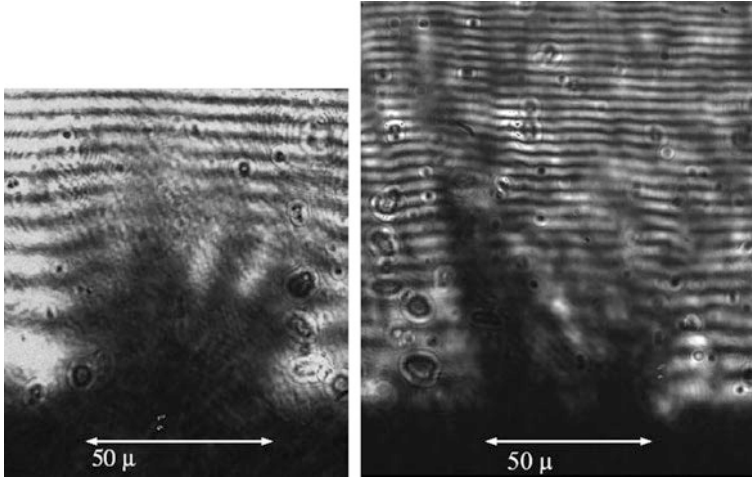
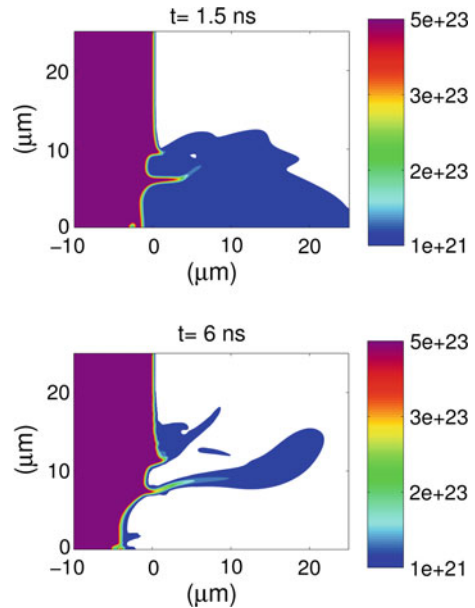


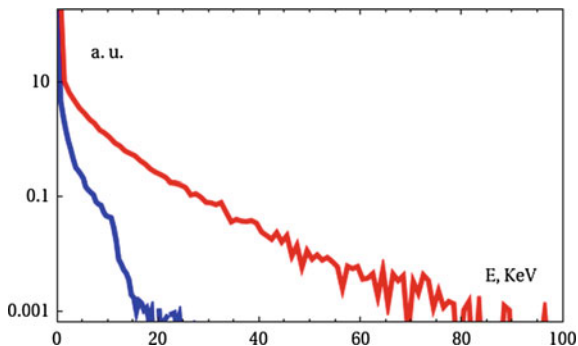
Fig. 2.3 Shadowgraphy images of jets produced by the pre-pulse acting at the melted gallium surface (intensity 10^{16} W/cm²): along the laser-beam direction (*left pane*) and in the perpendicular direction (*right pane*)

Fig. 2.4 2D hydrodynamic simulations of a liquid aluminum ablation. The energy density in the central spot (4 μm in diameter) was 14 J/cm², and in the outer ring (7.5 μm radius, width of 1 μm) it was few times less [4] (calculations by the group of Prof. V. Tikhonchuk)



To understand why interaction of the main laser pulse with jets leads to hard X-ray yield enhancement, we made 3D PIC simulations in tight collaboration with Prof. Bychenkov's group from the Lebedev Institute [2]. We observed that the long

Fig. 2.5 Electron spectra from plasma with (red line) and without (blue line) jets [5]



tail of hot electrons appears if we have jets and that means that those hot electrons are produced due to the existence of these jets (Fig. 2.5).

The main application of our designed source could be so-called phase-contrast imaging of biological tissues (see, for example [5]). Note that phase-contrast images are excellent if one needs to reveal the boundaries between weakly absorbing tissues. This method is extensively used with synchrotron-radiation sources, but our aim is to bring the process to a small-scale laboratory, thus providing for the feasibility to use this method in medicine.

The next part of the talk concerns γ -ray production, so here we are talking about X-rays with quantum energies well above 100 keV. Recently we tried [6] to understand how the real temporal structure of the pre-pulse impacts hard X-ray and γ -ray yields. The main outcome was that having really high contrast femtosecond pulse is not good and efficient for γ production, and a short pre-pulse, which comes 12 ns in advance (a more-or-less normal feature of femtosecond lasers with CPA), again is not good. It is much better to have long and arbitrarily intense amplified spontaneous emission, and then one has enhanced γ -ray yield.

Note that amplified spontaneous emission is not a good thing because you cannot control it, you cannot play with its intensity and its duration, and it is unstable from shot to shot. That is why we turned to a different scheme where we have a femtosecond laser pulse and we have a pre-pulse, which is artificial. Here we have the high-contrast femtosecond pulse and artificial pre-pulse, so we can control energy deposition by the pre-pulse, plasma-plume velocity, timing between the two pulses, and plume extent. We can use pre-pulse at 1064 or 532 nm, and that helps us with optical plasma diagnostics.

Our experimental scheme is presented in Fig. 2.6. The main pulse comes from the Ti:sapphire system, and the pre-pulse comes from the Q-switched Nd:YAG laser (Surelite III) with pulse duration of 6 ns. The latter produces intensities up to 10^{12} W/cm². We have various diagnostics around the chamber: γ -ray detectors, X-ray detectors, some visible diagnostics, and an optical spectrometer. We also have ionic diagnostics which is not shown here.

Figure 2.7a presents the dependence of the hard X-ray yield on the delay between the two pulses. Zero delay corresponds to the coincidence of the maxima

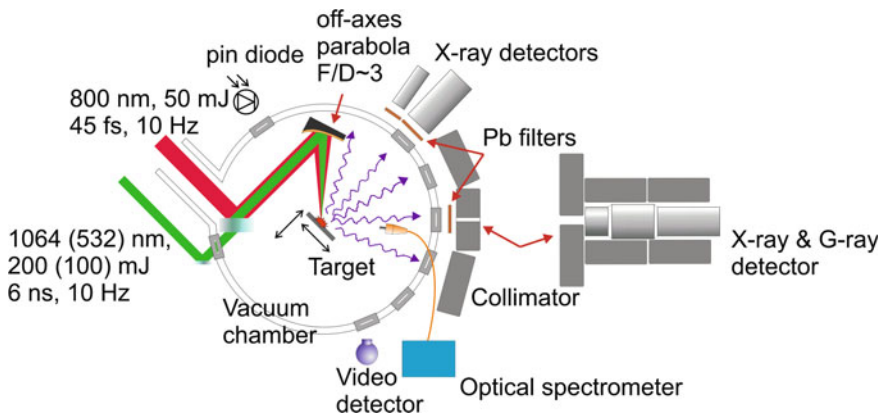


Fig. 2.6 Experimental scheme for γ -ray production

Fig. 2.7 γ -yield dependence on the time delay between the pre-pulse and the main pulse (a) and γ spectra at different delays (b)

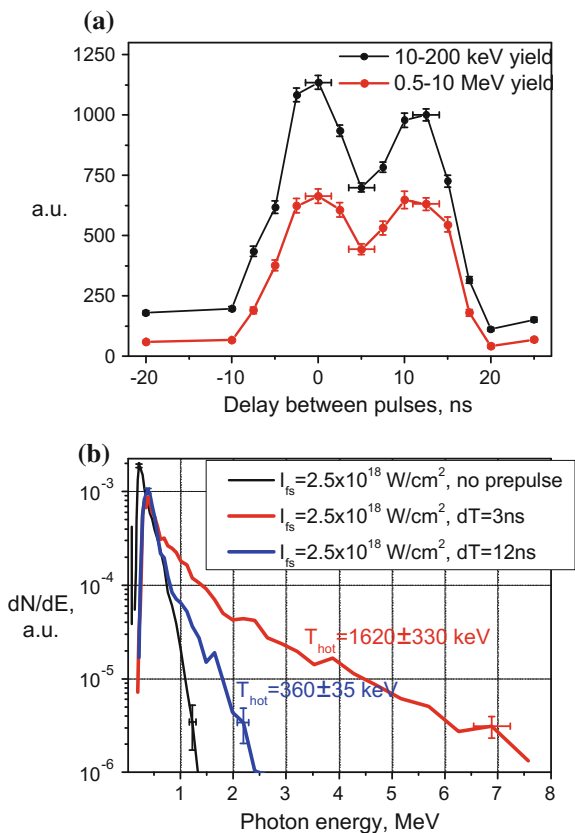
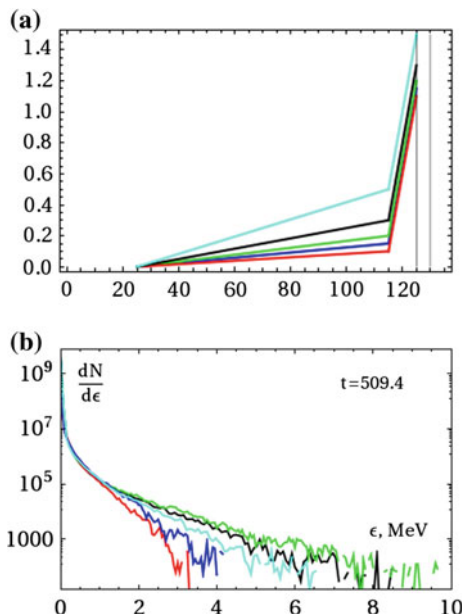


Fig. 2.8 Plasma densities used in 2D PIC modeling (a) and corresponding spectra of electrons (b)



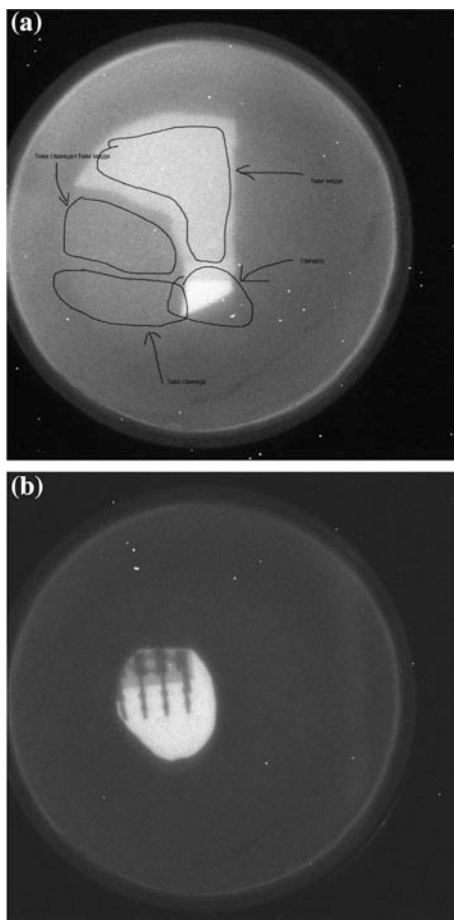
of two pulses, and negative delays means that the nanosecond pulse comes in advance with respect to the main pulse. One can see two maxima and a deep, so this is again indicating some interesting physics inside. For applications, the most interesting data are presented in Fig. 2.7b. The spectrum obtained with a properly timed pre-pulse generated many more gammas and the mean energy (slope of the curve) of those gammas is much higher. Surprisingly, at an intensity a little bit above 10^{18} W/cm^2 , we obtained few MeV photons (up to 7 MeV).

From optical diagnostics, we can assume that the laser-plasma plume looks like something presented in Fig. 2.8a: we have two slopes and a long tail of under-critical plasma. Spectra obtained with those slopes using 2D PIC simulations (Prof. Bychenkov group) are shown in Fig. 2.8b [7]. For some special slopes, we can optimize the hard X-ray yield.

Figure 2.9 shows X-ray images obtained with our source with most quanta having energy less than 1 MeV. Even though we can look inside microchips, or distinguish between different metallic foils and plates. In the future, our optimized source can be efficiently used for nuclear safety and non-proliferation issues, warm dense-matter diagnostics, etc.

This activity is supported by the Russian Fund for Basic Research under grants ##13-02-00373 and 16-02-00263 (γ -production and imaging), 14-29-09244 (electron acceleration in tenuous plasma), 15-32-20417 (X-ray phase imaging).

Fig. 2.9 γ -ray images of the filter set (*top*) and a microchip (*bottom*)



References

1. V.M. Gordienko, M.V. Kurilova, E.V. Rakov, A.B. Savel'ev-Trofimov, D.S. Uryupina, *Quantum Electron.* **37**, 651 (2007)
2. D.S. Uryupina, K.A. Ivanov, A.V. Brantov, A.B. Savel'ev, V. Yu. Bychenkov, M.E. Povarnitsyn, R.V. Volkov, V.T. Tikhonchuk, *Phys. Plasmas.* **19**, 013104 (2012)
3. K.A. Ivanov, D.S. Uryupina, R.V. Volkov, A.P. Shkurinov, I.A. Ozheredov, A.A. Paskhalov, N.V. Eremin, A.B. Savel'ev, Nuclear instruments and methods in physics research section a: accelerators, spectrometers, detectors and associated equipment. *Spec. Issue Superstrong 2010.* **653**, 58 (2011)
4. D.A. Lar'kin, K. Uryupina, A. Ivanov, T. Savel'ev, F. Bonnet, F. Gobet, M. Hannachi, M. Tarisien, K. Versteegen, K. Spohr, B. Breil, F. Chimier, C. Dorchies, *Phys. Plasmas* **21**, 093103 (2014)

5. R. Toth, J.C. Kieffer, S. Fourmaux, T. Ozaki, A. Krol, *Rev. Sci. Instrum.* **76**, 083701 (2005)
6. K.A. Ivanov, S.A. Shulyapov, P.A. Ksenofontov, I.N. Tsymbalov, R.V. Volkov, A.B. Savel'ev, A.V. Brantov, VYu. Bychenkov, A.A. Turiinge, A.M. Lapik, A.V. Rusakov, R.M. Djilkibaev, V.G. Nedorezov, *Phys. Plasmas* **21**, 093110 (2014)
7. K.A. Ivanov, S.A. Shulyapov, A.A. Turiinge, A.V. Brantov, D.S. Uryupina, R.V. Volkov, A.V. Rusakov, R.M. Djilkibaev, V.G. Nedorezov, *Contr. Plasma Phys.* **53**, 116 (2013)

Progress in Photon Science

Basics and Applications

Yamanouchi, K. (Ed.)

2017, XVII, 288 p. 235 illus., 201 illus. in color.,

Hardcover

ISBN: 978-3-319-52430-6